NANO LETTERS

pubs.acs.org/NanoLett

Letter

Weighing the DNA Content of Adeno-Associated Virus Vectors with Zeptogram Precision Using Nanomechanical Resonators

Georgios Katsikis,* Iris E. Hwang, Wade Wang, Vikas S. Bhat, Nicole L. McIntosh, Omair A. Karim, Bartlomiej J. Blus, Sha Sha, Vincent Agache, Jacqueline M. Wolfrum, Stacy L. Springs, Anthony J. Sinskey, Paul W. Barone, Richard D. Braatz, and Scott R. Manalis*

Cite This: *Nano Lett.* 2022, 22, 1511−1517

Read Online

ACCESS | Metrics & More | Article Recommendations | Supporting Information

ABSTRACT: Quantifying the composition of viral vectors used in vaccine development and gene therapy is critical for assessing their functionality. Adeno-associated virus (AAV) vectors, which are the most widely used viral vectors for in vivo gene therapy, are typically characterized using PCR, ELISA, and analytical ultracentrifugation which require laborious protocols or hours of turnaround time. Emerging methods such as charge-detection mass spectroscopy, static light scattering, and mass photometry offer turnaround times of minutes for measuring AAV mass using optical or charge properties of AAV. Here, we demonstrate an orthogonal method where suspended nanomechanical resonators (SNR) are used to directly measure both AAV mass and aggregation from a few microliters of sample within minutes. We achieve a precision near 10 zeptograms which corresponds to 1% of the genome holding capacity of the AAV capsid. Our results show the potential of our method for providing real-time quality control of viral vectors during biomanufacturing.

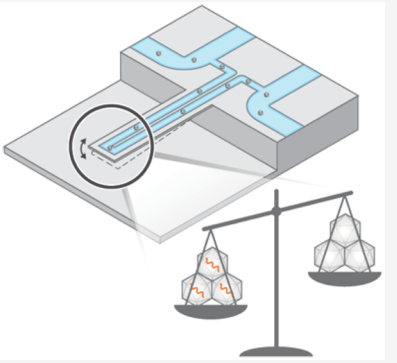

KEYWORDS: *nanofluidics, mechanical resonators, gene therapy, nanoparticles, viral vectors, AAV*

Adeno-associated viruses (AAV) are the most widely used viral vectors for in vivo gene therapy due to their nonpathogenicity, low immunogenicity, and long-term gene expression.[1] However, AAV biomanufacturing is inefficient, producing only a small percentage (5−30%) of capsids containing the therapeutic gene; the majority of the produced capsids are empty which decreases the efficacy of gene therapy, increases its cost,[2,3] and has safety considerations.[4]

To increase the efficiency of AAV biomanufacturing, it is critical to provide real-time quality control to the process. As quality control is limited when using traditional molecular biology methods PCR and ELISA, in part due to their long turnaround times,[5] emerging methods based on mass measurement provide faster readouts for assessing the ratio of full (or "heavy") to empty (or "light") AAV capsids. In particular, mass spectrometers have been enhanced to independently measure mass through charge detection,[6−9] achieving attogram (or MDa) resolution. Multiangle static light scattering detectors optically measure mass with subattogram (or kDa) resolution.[10,11] More recently, microscopy-based methods correlating interferometric contrast and mass have also achieved kDa mass resolution.[12−14] These methods offer potential for real-time quality control and, although they depend on the optical or charge properties of a given AAV sample, this dependence is addressed by using standard protein calibrants with corrections for nucleic acids.[15]

Here, we directly measured AAV mass using mechanical resonators.[16] In particular, we used suspended nanochannel resonators[17] (SNR) to weigh AAVs in solution by measuring their buoyant mass, referred to from this point on as "mass" (Figure 1a). The SNR is a hollow cantilever driven to vibrate at its resonant frequency f; when a single particle, such as a virus, flows through the cantilever, the resonant frequency of the cantilever transiently changes by Δf_s in proportion to the particle's mass.[18] Notably, the optical or charge properties of the virus do not affect the readout signal Δf_s, thus the resonators are routinely calibrated with a solution of particles with reference mass.[18]

We previously used this approach to measure the mass of gold nanoparticles down to 10 nm in diameter[19] corresponding to a mass of 10 ag. However, a single AAV has a mass of 1−2 ag (molecular weight of MW_{AAV} = 3.8−5.4 MDa,[20−22] Supporting Information S1), thus the frequency change Δf_s from a single AAV is occluded by noise. Although nanomechanical resonators have the potential to weigh single AAVs in a vacuum environment,[23] weighing AAVs in aqueous solution would enable rapid turnaround times which are ultimately required for real-time quality control.

Received: October 25, 2021
Revised: February 3, 2022
Published: February 11, 2022

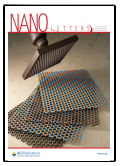

https://doi.org/10.1021/acs.nanolett.1c04092
Nano Lett. 2022, 22, 1511−1517

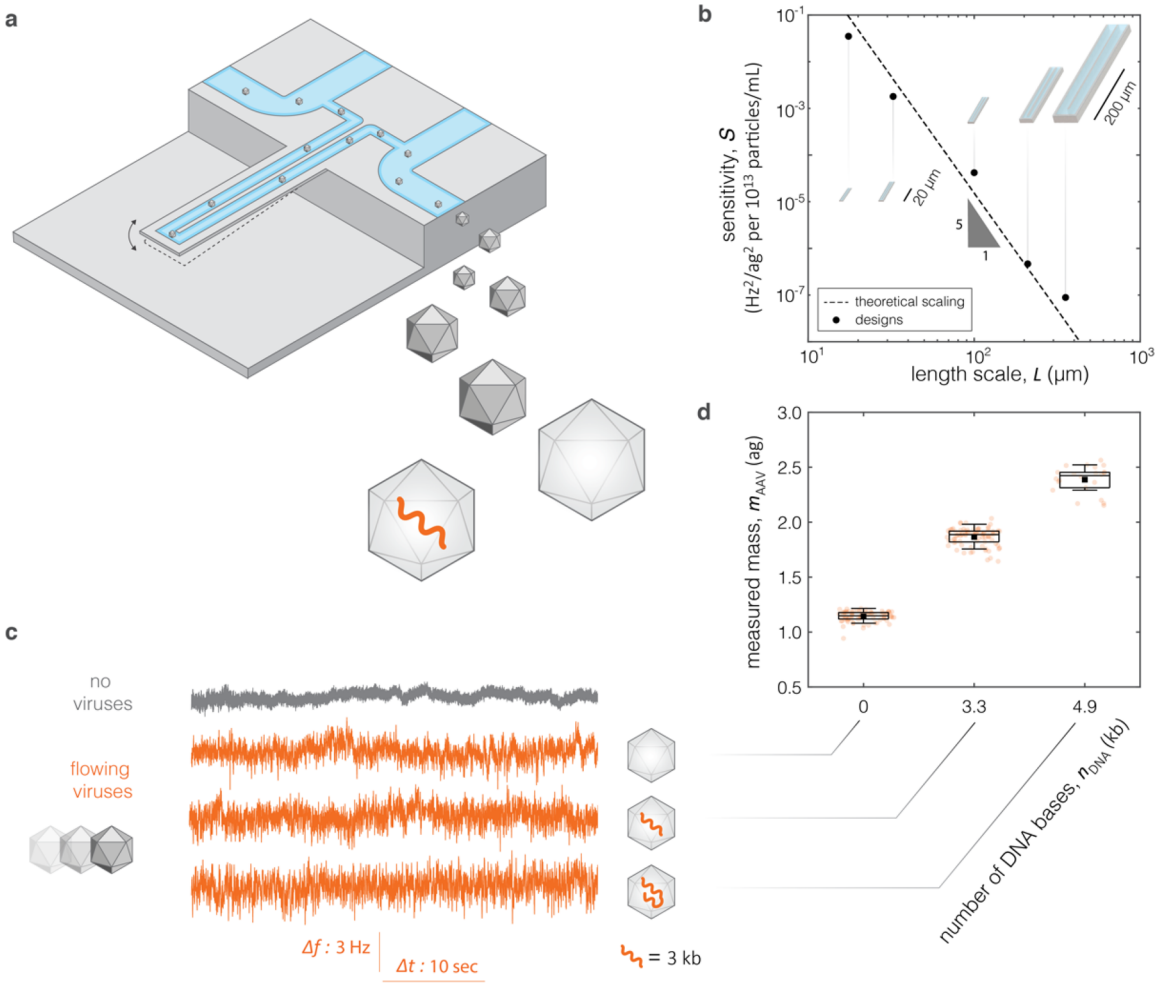

Figure 1. Concept of measuring mass of AAVs in solution. (a) Schematic of SNR featuring a hollow cantilever of length $L = 17.5\ \mu$m that vibrates at first resonant mode with frequency f. Inside the cantilever, we flowed solutions of AAVs with different DNA content or genetic constructs (denoted by orange color). (b) Sensitivity S of root-mean-square Δf_{rms} of signal $\Delta f(t)$ versus length scale L of cantilever. Sensitivity is in units of Hz^2 per nanoparticles of 1 ag buoyant mass at a concentration of 10^{13} particles/ml. Dashed line and triangle denote theoretical scaling with length $S \sim L^{-5}$, and black points represent experimental designs (Supporting Information S4). (c) Experimental time-series signals of change $\Delta f(t)$ of resonant frequency exclusively due to noise in the absence of AAVs (gray) and due to flowing AAVs with distinct genetic constructs, having nominal number n_{DNA} of DNA kilobases (kb), $n_{DNA} = 0$, 3.3, 4.9 kb (from top to bottom in orange). (d) Measured mass m_{AAV} of AAVs calculated from time-series data of panel c versus n_{DNA}. Each point represents an analyzed time-series trace of 30 sec. The central marks and black squares respectively indicate the median and mean. The bottom and top edges of the boxes respectively indicate the 25th and 75th percentiles. The bottom and top whiskers indicate the 5th and 95th percentiles. Percentiles are defined by assuming points follow normal distributions.

To circumvent the noise limit for weighing single AAVs in solution, we flowed AAV samples at concentrations of 10^{12}–10^{13} particles/ml such that tens to hundreds of AAVs simultaneously flow through the resonator (Figure 1a). This results in a complex time-series signal of frequency change $\Delta f(t)$ which contains information about the average mass of the particles as well as the characteristics of the flow. This concept has previously been used in microchannel resonators[24,25] to measure the mass of polystyrene and gold nanoparticles weighing 20 ag, which are an order of magnitude heavier than AAVs. In addition, the signal $\Delta f(t)$ also measures the volume of the particles[25] in an approach similar to dynamic light scattering.[26] Here, we scaled down the resonators from the micro- to nanoscale and used spectral denoising to enable mass measurement of AAVs in the concentration range of 10^{12}–10^{13} particles/mL achieving a precision near 10 zeptograms (zg) in a 10 min sampling window.

To enable measurement of AAV mass, we first theoretically characterized the root-mean-square Δf_{rms} of signal $\Delta f(t)$ as a function of the properties of the resonator in the form of a vibrating cantilever. It has been shown that Δf_{rms} (equivalent to the variance σ^2 when the mean is $\mu = 0$) is proportional to the product cm_{np}^2 of average concentration c and average mass m_{np} of nanoparticles.[24] Here, we derived $\Delta f_{rms} = Scm_{AAV}^2$ where m_{AAV} is the average mass of AAV nanoparticles, and the sensitivity $S = f^2 a_V V/(4m_{eff}^2)$ depends on the resonance frequency f, the volume V of the fluid channel, the effective mass m_{eff} of the cantilever,[18] and the volume utilization factor a_V related to the resonant mode n_m and the dimensions of the cantilever (Figure 1b, Supporting Information S2, S3, S4). The sensitivity, S, for a length scale, L, of the cantilever scales as $S \sim L^{-5}$ (Figure 1b, Supporting Information S2) indicating that the smaller the cantilever, the greater the Δf_{rms}. On the basis of the scaling of S and the availability of previously characterized cantilevers,[27] we used the one with the smallest length $L = 17.5$

https://doi.org/10.1021/acs.nanolett.1c04092
Nano Lett. 2022, 22, 1511−1517

μm, a fluid channel with a cross-sectional area 700 × 700 nm^2, and a baseline resonant frequency $f \cong 4.5$ MHz (Supporting Information S4).

Next, we measured AAV solutions with distinct genetic constructs, having nominal number n_{DNA} of DNA kilobases (kb), n_{DNA} = 0, 3.3, and 4.9 kb (Supporting Information S5). In the context of this study, we characterized the AAV5 serotype which is less prone to aggregation than AAV2 which is most commonly used in gene therapy.[28] Prior to testing, our AAV solutions were filtered and their purity was verified with SDS-PAGE and InstantBlue Staining (Supporting Information S5). When flowing these AAV samples in the SNR, we measured signals of frequency change $\Delta f(t)$ which were visually distinct from the baseline noise (Figure 1c). Furthermore, we calculated the mass m_{AAV} from the signals $\Delta f(t)$ and found that the measured mass for each AAV sample is distinguishable from one another (Figure 1d).

To validate our measurements, we performed experiments with nanoparticles of known mass as a reference standard for calibration. In particular, we used gold nanoparticles of nominal diameter $d_{Au,nom}$ = 5 nm (Supporting Information S5). Using dynamic light scattering (DLS) we measured their mean hydrodynamic diameter and converted it to reference mass of $m_{Au,ref}$ = 1.51 ag which is similar to that of AAV (Supporting Information S6). Furthermore, to gain insight into the experimental measurements, we developed a computational model based on the advection and diffusion of nanoparticles as they transit through the cantilever via a laminar flow, determined by a low Reynolds number[29] (Supporting Information S7, Video S1). However, when we flowed gold nanoparticles in the cantilever, we found that calculating Δf_{rms} in the presence of noise overpredicts the nanoparticle mass (m_{Au} > 2 ag) in both the experiments and simulations (Figure 2, gray).

To correct for the overprediction of nanoparticle mass, we first simulated the "pure" signal $\Delta f(t)$ caused by the flow of nanoparticles inside the cantilever in the absence of noise. We found that $\Delta f(t)$ in the frequency domain is well-represented by a canonical Gaussian form $e^{-\delta\xi^2}$, and when we calculated Δf_{rms} using a Gaussian fit in the frequency domain we correctly predicted the nanoparticle mass (Supporting Information S8). We then experimentally characterized the noise in our system in the frequency domain and identified a canonical form $1/\xi^a$ of colored noise where ξ represents the spectral frequency, and the decay factor a lies in the range a = 1−2 (Supporting Information S9). Combining the canonical forms for "pure" signal and noise, we developed a spectral denoising method that calculates Δf_{rms} in the frequency domain while neutralizing the effect of noise (Supporting Information S9). By applying spectral denoising to experiments and simulations of gold nanoparticles, we obtained results which are consistent with those obtained from dynamic light scattering (Figure 2, blue and red). Remarkably, the spectral denoising method applied to data from both the experiments and simulations leads to a measurement precision of 10−100 zg (1 zg = 10^{-3} ag), defined here as the standard error calculated over a 10 min sampling window for concentrations of c = 5−20 × 10^{12} particles/ml (Supporting Information S10).

To obtain a validation of our AAV measurements with the SNR, we first used established methods for characterizing AAVs[5,30] (Supporting Information S5). Specifically, we characterized an AAV sample encompassing a genetic construct of green fluorescent protein (GFP) with a nominal number n_{DNA} = 3.3 kb using alkaline agarose gel electrophoresis (AAGE) and analytical ultracentrifugation (AUC) (Figure 3a,b). AAGE revealed the presence of two distinct DNA bands; the "heavy" (2.8 kb) is close to the nominal number of the construct, and the "heavy cs" (4.7 kb) likely corresponds to a maximum-size construct that can be packaged inside the capsid as a result of an unintended formation of a self-complementary (cs) DNA sequence[31] (Figure 3a). AUC and AAGE consistently revealed the presence of these two constructs. In addition, AUC identified residual DNA, "light" (∼0 kb) and "intermediate" (<3.3 kb) capsids as well as aggregates (Figure 3b, Supporting Information S11).

We found that Δf_{rms} from SNR method (Figure 3d) measures AAV mass that is consistent with the results from AAGE and AUC. By using spectral denoising (Supporting Information S9), simulations (Supporting Information S7) and conversions of measured AAV mass to DNA content (Supporting Information S1), our measurements are within the margin specified by AUC (Figure 3d). In addition, our results are consistent with static light scattering (SLS) measurements, an orthogonal method recently used for characterizing AAVs[11] (Figure 3d, Supporting Information S12). Overall, we found that our SNR measurements are reliable down to a concentration limit of $c \cong 5 \times 10^{12}$ particles/ml (Figure 3d). Below that limit, the contribution of noise to Δf_{rms} is higher than that of the AAV signal (Supporting Information S13). Notably, the precision of AAV mass measurements, similar to that of gold nanoparticles (Figure 2), is maintained at a near 10 zg level at the upper

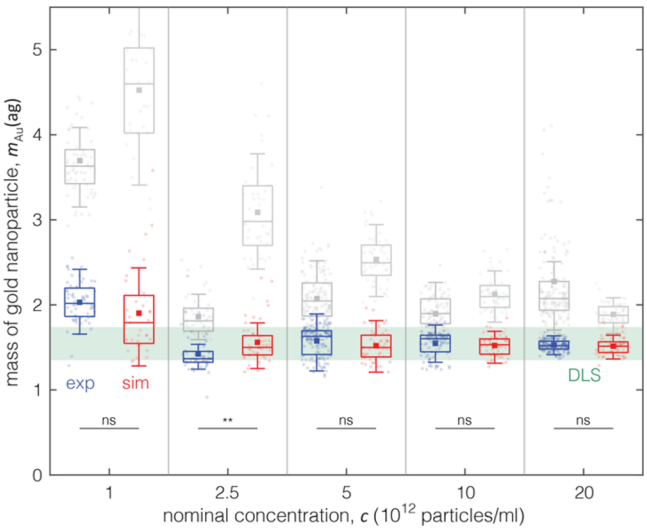

Figure 2. Validation of SNR measurements using nanoparticles of known mass. Mass of gold nanoparticles of nominal diameter $d_{Au,\ nom}$ = 5 nm versus nominal concentration c (nonlinear scale) specified with or without spectral denoising in experiments (exp, blue or gray) and simulations (sim, red or gray) (Supporting Information S9). When spectral denoising is used, the mass measurements from experiments and simulations are independent of concentration and consistent with the results from DLS (green band) revealing a mass of $m_{Au,ref}$ = 1.51 ag corresponding to hydrodynamic diameter of d = 5.4 nm (Supporting Information S6). Box plots have similar notations as in Figure 1. The symbol * denotes $p < 0.05$, ** denotes $p < 0.01$ for the t test, and *ns* denotes nonsignificant difference between experiments and simulations.

https://doi.org/10.1021/acs.nanolett.1c04092
Nano Lett. 2022, 22, 1511−1517

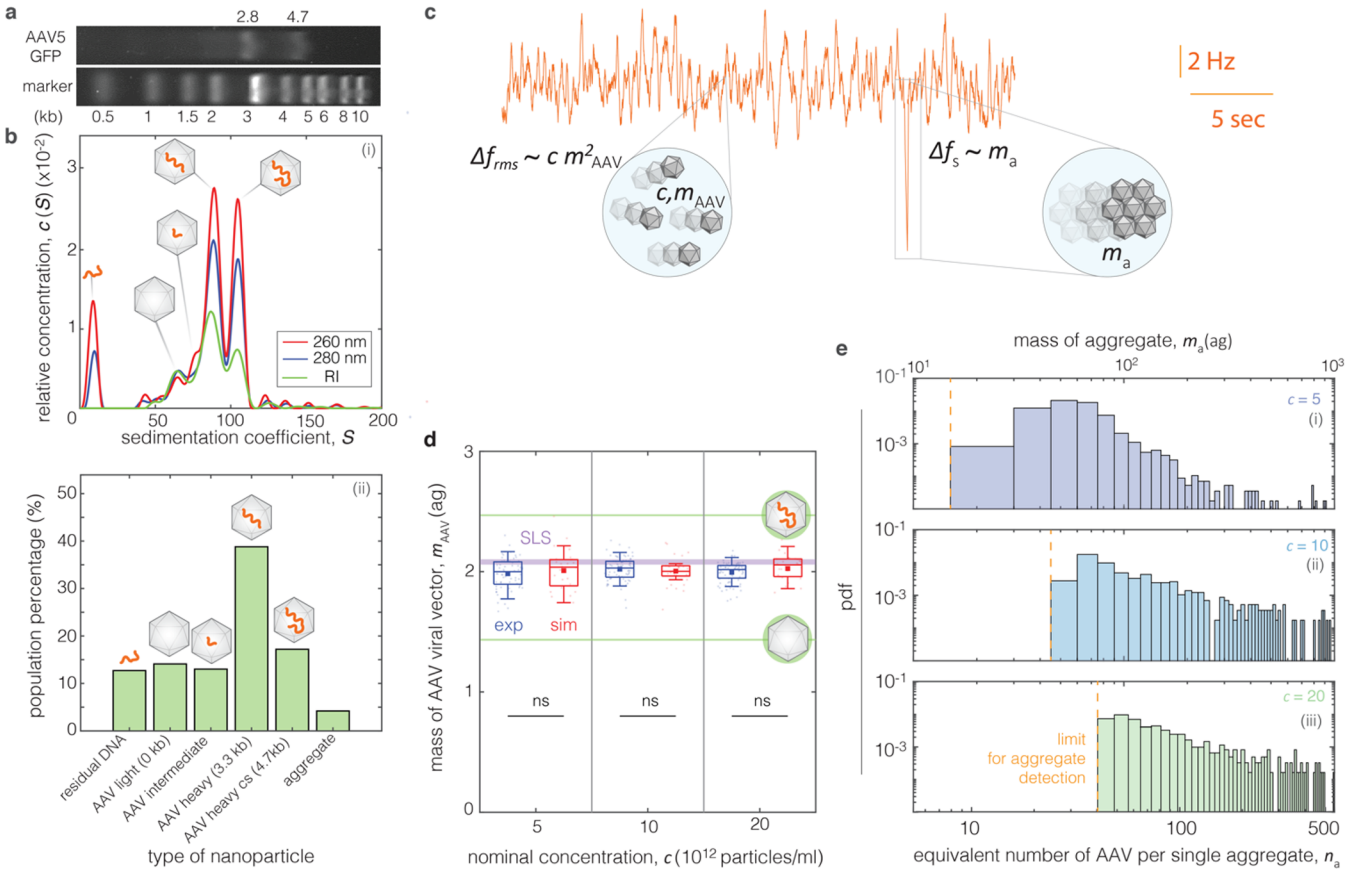

Figure 3. Measuring AAV mass and aggregation. (a) alkaline gel electrophoresis (AAGE) analysis of AAV-GFP (top) versus marker (bottom) measuring number of DNA bases (kb). (b) Analytical ultracentrifugation (AUC) analysis of AAV-GFP using refractive index (RI) signal (green) and 260, 280 nm UV wavelengths (red, blue) (i). $c_{260}/c_{280} > 1$ indicates AAV capsids filled with DNA[26] (e.g., "heavy capsids".) Population percentage (ii) extracted from (i) with numbers corresponding to peaks indicating different types of AAV (insets). The letters "cs" in "AAV heavy cs" denote complementary strand, filling up the capsid to its maximum holding capacity (4.7 kb) (c) Example of experimental signal $\Delta f(t)$ showing the simultaneous measurements of the average AAV mass m_{AAV} of concentration c (Δf_{rms}), and the mass m_a of individual aggregates ($\Delta f_s < 0$). Box plots have similar notation as in Figures 1 and 2. (d) Mass m_{AAV} of AAV viral vector with genetic construct of GFP versus nominal concentration c (nonlinear scale) measured using spectral denoising in both experiments (exp, blue) and simulations (sim, red). The purple band indicates the range of mass specified using static light scattering (SLS) where its width is standard deviation from $n = 3$ experiments. The green bands correspond to the types of AAV from panel b. (e) Probability density functions of mass m_a of aggregates (top horizontal axis), also expressed as equivalent number of AAVs per single aggregates (bottom horizontal axis) for three concentrations (i–iii). The limit for detection of aggregates (orange) is governed by Δf_{rms} being dependent on c.

concentration range of $c = 2 \times 10^{13}$ particles/mL (Supporting Information S10).

Simultaneously with measuring AAV mass, we determined the mass m_a of single aggregates, each of which manifests as a transient decrease in resonant frequency (Figure 3c, $\Delta f_s < 0$) as each aggregate passes through the cantilever. As a basis for comparison, we confirmed the presence of soluble aggregates in our AAV sample using DLS although DLS cannot in principle resolve the heterogeneity of aggregates (Supporting Information S6). The presence of aggregates was not only evident in analytical ultracentrifugation (Figure 3b) but also in chromatographic methods. In particular, anion exchange chromatography analysis (AEX)[32] exhibited long tailing at higher elution times (Supporting Information S14) while size exclusion chromatography (SEC) showed long tailing at the lower elution times (Supporting Information S15). Using SNR, we directly measured the mass of these single aggregates and characterized their heterogeneity (Figure 3e). Importantly, the detection limit for weighing single aggregates by our method depends on the baseline frequency noise of $\Delta f(t)$ which is essentially governed by Δf_{rms}, being dependent on the AAV concentration (Supporting Information S8). However, within the limits of aggregate detection, we found that the mass heterogeneity of aggregates was similar for the three tested AAV concentrations in the range $c = 5–20 \times 10^{12}$ particles/ml (Figure 3e).

We leveraged the measurement of AAV mass to convert our readout to a ratio of full to empty or "heavy to light" capsids which, along with aggregation, is a critical quality attribute of a given AAV product.[5] We thus measured the mass of AAV mixtures with different volume ratios of AAV heavy as AAV-GFP ($n_{DNA} = 3.3$ kb) and AAV light as AAV-empty without a nominal DNA construct ($n_{DNA} = 0$ kb). We observed that our experimental results are consistent with our simulations with a trend of increasing mass for mixtures of higher percentage of heavy-to-light capsids (Figure 4a). In addition, given the theoretical mass values for AAVs based on their DNA content, (Supporting Information S1), we converted the mass m_{AAV} to percentage of heavy AAV capsids, obtaining consistent percentages with those determined by static light scattering for the same mixture ratios (Figure 4b).

https://doi.org/10.1021/acs.nanolett.1c04092
Nano Lett. 2022, 22, 1511–1517

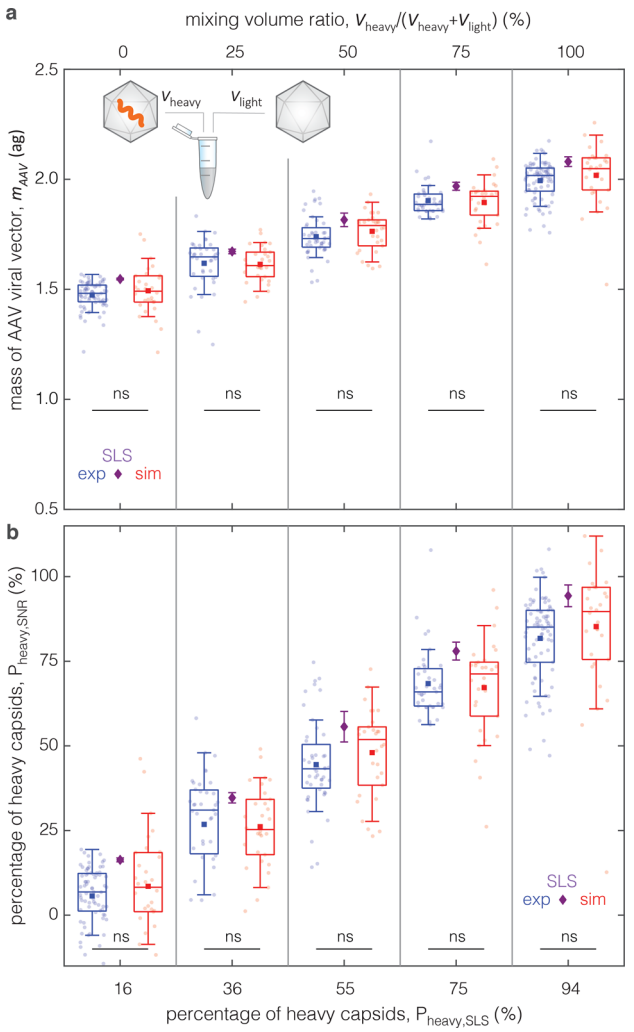

Figure 4. Calculation of percentage of heavy capsids using mass measurement of AAV. (a) Mass m_{AAV} of mixtures of two types of AAV samples: (i) GFP heavy and (ii) empty light versus mixing volume ratio for experiments (exp, blue) simulations (sim, red). (b) Percentage of heavy capsids, defined as $P_{heavy} = (m_{AAV} - m_{light})/(m_{heavy} - m_{light})$ for SNR (vertical axis) versus SLS (horizontal axis) where m_{light}, m_{heavy} are theoretical values for buoyant mass of AAV (Supporting Information S1) when they respectively contain no DNA (n_{DNA} = 0 kb) or DNA of the genetic construct of GFP (n_{DNA} = 3.3 kb). The horizontal axis corresponds to the percentage of full capsids calculated using SLS, also denoted by purple diamonds. Error bars denote standard deviation in SLS experiments (n = 3 per mixing volume ratio). Boxplots have similar notation as in Figures 1, 2, and 3.

Our SNR results establish the foundations for a real-time method for characterizing AAV-based viral vectors in solution. It requires minimal amount of sample (1−5 μL) and as a flow-through method, it is amenable for integration with manufacturing unit operations for online characterization of AAV products. Importantly, it simultaneously and within minutes quantifies both the average DNA context and individual aggregates, which constitute two critical quality attributes of a given AAV product.[5]

In addition to SNR, characterization methods such as analytical ultracentrifugation, charge-detection mass spectroscopy, mass photometry, or light scattering rely on different principles to measure DNA content of AAV with distinct strengths and limitations.[5] Therefore, we envision that the success of AAV characterization will rely on a synergistic pipeline of multiple orthogonal methods that provide different signal detection readouts. Preceding this downstream characterization, upstream purification is equally important to minimize biases due to the presence of impurities.[5] In particular, chromatography-based methods, such as size exclusion or anion exchange chromatography remain indispensable elements of the overall pipeline of AAV characterization[5,11,33,34] despite their limitations in resolving capsid heterogeneity. Such characterization coupled with molecular engineering, process development,[35] as well as mathematical modeling/simulation[36] of the AAV biomanufacturing process may lead to new paradigms for scaling up production of viral vectors. Although our approach is showcased here for AAV, we envision it is also applicable to a broader context of viral vectors, thereby paving the ground for increasing the efficacy of gene therapy treatments while maintaining their affordability and clinical safety.

■ ASSOCIATED CONTENT

Supporting Information

The Supporting Information is available free of charge at https://pubs.acs.org/doi/10.1021/acs.nanolett.1c04092.

Detailed information on supporting figures, theory, and methods (PDF)

Video S1 showing simulation of adeno-associated viruses flowing through suspended nanochannel resonator (top) with resulting signal of change in resonant frequency $\Delta f(t)$ as viruses are flowing through the resonator (bottom) (MP4)

■ AUTHOR INFORMATION

Corresponding Authors

Georgios Katsikis − *Koch Institute for Integrative Cancer Research, Massachusetts Institute of Technology, Cambridge, Massachusetts 02139, United States;* orcid.org/0000-0003-3239-4924; Email: geokats@mit.edu, katsikis.g@gmail.com

Scott R. Manalis − *Koch Institute for Integrative Cancer Research, Department of Mechanical Engineering, and Department of Biological Engineering, Massachusetts Institute of Technology, Cambridge, Massachusetts 02139, United States;* orcid.org/0000-0001-5223-9433; Email: srm@mit.edu

Authors

Iris E. Hwang − *Koch Institute for Integrative Cancer Research, Massachusetts Institute of Technology, Cambridge, Massachusetts 02139, United States;* Present Address: Pioneer Natural Resources, Irving, Texas 75038, United States; orcid.org/0000-0001-9223-8187

Wade Wang − *BioMarin Pharmaceutical, Inc., Novato, California 94949, United States;* orcid.org/0000-0002-7639-2122

Vikas S. Bhat − *BioMarin Pharmaceutical, Inc., Novato, California 94949, United States*

Nicole L. McIntosh − *BioMarin Pharmaceutical, Inc., Novato, California 94949, United States*

Omair A. Karim − *BioMarin Pharmaceutical, Inc., Novato, California 94949, United States*

https://doi.org/10.1021/acs.nanolett.1c04092
Nano Lett. 2022, 22, 1511−1517

Bartlomiej J. Blus − *BioMarin Pharmaceutical, Inc., San Rafael, California 94901, United States;* orcid.org/0000-0002-6979-0851

Sha Sha − *Center for Biomedical Innovation, Massachusetts Institute of Technology, Cambridge, Massachusetts 02139, United States;* Present Address: Ultragenyx, Cambridge, Massachusetts 02139, United States.; orcid.org/0000-0002-4514-5671

Vincent Agache − *Université Grenoble Alpes, CEA, LETI, 38000 Grenoble, France;* orcid.org/0000-0001-7796-9467

Jacqueline M. Wolfrum − *Center for Biomedical Innovation, Massachusetts Institute of Technology, Cambridge, Massachusetts 02139, United States*

Stacy L. Springs − *Center for Biomedical Innovation, Massachusetts Institute of Technology, Cambridge, Massachusetts 02139, United States;* orcid.org/0000-0003-2133-5689

Anthony J. Sinskey − *Center for Biomedical Innovation and Department of Biology, Massachusetts Institute of Technology, Cambridge, Massachusetts 02139, United States;* orcid.org/0000-0002-1015-1270

Paul W. Barone − *Center for Biomedical Innovation, Massachusetts Institute of Technology, Cambridge, Massachusetts 02139, United States;* orcid.org/0000-0001-6802-6846

Richard D. Braatz − *Center for Biomedical Innovation and Department of Chemical Engineering, Massachusetts Institute of Technology, Cambridge, Massachusetts 02139, United States;* orcid.org/0000-0003-4304-3484

Complete contact information is available at: https://pubs.acs.org/10.1021/acs.nanolett.1c04092

Author Contributions

G.K. and S.R.M. conceived the study. G.K., W.W., V.S.B., and S.R.M. designed the research. G.K. carried out the theoretical analysis and performed the experiments with the suspended nanochannel resonators. V.A. provided the suspended nanochannel resonators. I.E.H. developed the computational model. G.K. and I.E.H. performed the simulations. S.S. did initial PCR and ELISA measurements and supported the early development of the project. W.W., N.L.M., O.A.K., and B.J.B. performed the experiments using established methods for characterizing AAVs. G.K., I.E.H. N.L.M., O.A.K., B.J.B., and W.W. analyzed the results. V.S.B., V.A., J.M.W., S.L.S., A.J.S., P.W.B., R.D.B., and S.R.M. guided the work. G.K., I.E.H., W.W., and S.R.M. wrote the paper with feedback from V.S.B., V.A., J.M.W., S.L.S., A.J.S., P.W.B, B.J.B., and R.D.B.

Funding

This study is supported by a grant from the U.S. Food and Drug Administration (Grant ID 1R01FD006584-02, Continuous Viral Vector Manufacturing based on Mechanistic Modeling and Novel Process Analytics). This study is also supported by a grant from the Massachusetts Life Science Center as part of the Building Breakthroughs program. S.R.M. and G.K. acknowledge support from the Virginia and D.K. Ludwig Fund for Cancer Research.

Notes

The authors declare the following competing financial interest(s): S.R.M. is a co-founder of Travera and Afnity Biosensors, which develops technologies relevant to the research presented in this work.

■ ACKNOWLEDGMENTS

We acknowledge Julie Sutton for discussion on noise characterization and help with experimental configurations of the suspended nanochannel resonator. We acknowledge Betsy Skrip from MIT Center for Biomedical Innovation for supporting the design of the figures.

■ REFERENCES

(1) Li, C.; Samulski, R. J. Engineering adeno-associated virus vectors for gene therapy. *Nat. Rev. Genet.* **2020**, *21*, 255−272.
(2) Clément, N.; Grieger, J. C. Manufacturing of recombinant adeno-associated viral vectors for clinical trials. *Mol. Ther. - Methods Clin. Dev.* **2016**, *3*, 16002.
(3) Kimura, T.; Ferran, B.; Tsukahara, Y.; Shang, Q.; Desai, S.; Fedoce, A.; Pimentel, D. R.; Luptak, I.; Adachi, T.; Ido, Y.; Matsui, R.; Bachschmid, M. M. Production of adeno-associated virus vectors for in vitro and in vivo applications. *Sci. Rep.* **2019**, *9*, 1−13.
(4) Mullard, A. Gene therapy community grapples with toxicity issues, as pipeline matures. *Nat. Rev. Drug Discovery* **2021**, *20*, 804−805.
(5) Gimpel, A. L.; et al. Analytical Methods for Process and Product Characterization of Recombinant Adeno-Associated Virus-based Gene Therapies. *Mol. Ther. - Methods Clin. Dev.* **2021**, *20*, 740−754.
(6) Pierson, E. E.; Keifer, D. Z.; Asokan, A.; Jarrold, M. F. Resolving Adeno-Associated Viral Particle Diversity with Charge Detection Mass Spectrometry. *Anal. Chem.* **2016**, *88*, 6718−6725.
(7) Todd, A. R.; Barnes, L. F.; Young, K.; Zlotnick, A.; Jarrold, M. F. Higher Resolution Charge Detection Mass Spectrometry. *Anal. Chem.* **2020**, *92*, 11357−11364.
(8) Wörner, T. P.; et al. Resolving heterogeneous macromolecular assemblies by Orbitrap-based single-particle charge detection mass spectrometry. *Nat. Methods* **2020**, *17*, 395−398.
(9) Wörner, T. P.; Snijder, J.; Friese, O.; Powers, T.; Heck, A. J. R. Assessment of genome packaging in AAVs using Orbitrap-based charge-detection mass spectrometry. *Mol. Ther. - Methods Clin. Dev.* **2022**, *24*, 40−47.
(10) Wyatt, P. J. Measurement of special nanoparticle structures by light scattering. *Anal. Chem.* **2014**, *86*, 7171−7183.
(11) McIntosh, N. L.; Berguig, G. Y.; Karim, O. A.; Cortesio, C. L.; De Angelis, R.; Khan, A. A.; Gold, D.; Maga, J. A.; Bhat, V. S. Comprehensive characterization and quantification of adeno associated vectors by size exclusion chromatography and multi angle light scattering. *Sci. Rep.* **2021**, *11*, 1−12.
(12) Cole, D.; Young, G.; Weigel, A.; Sebesta, A.; Kukura, P. Label-Free Single-Molecule Imaging with Numerical-Aperture-Shaped Interferometric Scattering Microscopy. *ACS Photonics* **2017**, *4*, 211−216.
(13) Young, G.; et al. Quantitative mass imaging of single molecules in solution. *Science* **2018**, *360*, 423−427.
(14) Wu, D.; Hwang, P.; Li, T.; Piszczek, G. Rapid Characterization of AAV gene therapy vectors by Mass Photometry. *Gene Ther.* **2022**, DOI: 10.1038/s41434-021-00311-4.
(15) Li, Y.; Struwe, W. B.; Kukura, P. Single molecule mass photometry of nucleic acids. *Nucleic Acids Res.* **2020**, *48*, E97.
(16) Burg, T. P.; et al. Weighing of biomolecules, single cells and single nanoparticles in fluid. *Nature* **2007**, *446*, 1066−1069.
(17) Gagino, M.; et al. Suspended Nanochannel Resonator Arrays with Piezoresistive Sensors for High-Throughput Weighing of Nanoparticles in Solution. *ACS Sensors* **2020**, *5*, 1230−1238.
(18) Dohn, S.; Svendsen, W.; Boisen, A.; Hansen, O. Mass and position determination of attached particles on cantilever based mass sensors. *Rev. Sci. Instrum.* **2007**, *78*, 103303.
(19) Olcum, S.; et al. Weighing nanoparticles in solution at the attogram scale. *Proc. Natl. Acad. Sci. U. S. A.* **2014**, *111*, 1310−1315.
(20) Torikai, K.; Ito, M.; Jordan, L. E.; Mayor, H. D. Properties of Light Particles Produced During Growth of Type 4 Adeno-Associated Satellite Virus. *J. Virol.* **1970**, *6*, 363−369.

(21) Rayaprolu, V.; et al. Comparative Analysis of Adeno-Associated Virus Capsid Stability and Dynamics. *J. Virol.* **2013**, *87*, 13150−13160.
(22) Govindasamy, L.; et al. Structural Insights into Adeno-Associated Virus Serotype 5. *J. Virol.* **2013**, *87*, 11187−11199.
(23) Chaste, J.; et al. A nanomechanical mass sensor with yoctogram resolution. *Nat. Nanotechnol.* **2012**, *7*, 301−304.
(24) Modena, M. M.; Wang, Y.; Riedel, D.; Burg, T. P. Resolution enhancement of suspended microchannel resonators for weighing of biomolecular complexes in solution. *Lab Chip* **2014**, *14*, 342−350.
(25) Modena, M. M.; Burg, T. P. Mass correlation spectroscopy for mass- and size-based nanoparticle characterization in fluid. *J. Appl. Phys.* **2015**, *118*, 224901.
(26) Stetefeld, J.; McKenna, S. A.; Patel, T. R. Dynamic light scattering: a practical guide and applications in biomedical sciences. *Biophys. Rev.* **2016**, *8*, 409−427.
(27) Katsikis, G.; Collis, J. F.; Knudsen, S. M.; Agache, V.; Sader, J. E.; Manalis, S. R. Inertial and viscous flywheel sensing of nanoparticles. *Nat. Commun.* **2021**, *12*, 5099.
(28) Wright, J. F.; et al. Identification of factors that contribute to recombinant AAV2 particle aggregation and methods to prevent its occurrence during vector purification and formulation. *Mol. Ther.* **2005**, *12*, 171−178.
(29) Stone, H. A.; Stroock, A. D.; Ajdari, A. Engineering flows in small devices: Microfluidics toward a lab-on-a-chip. *Annu. Rev. Fluid Mech.* **2004**, *36*, 381−411.
(30) Sommer, J. M.; et al. Quantification of adeno-associated virus particles and empty capsids by optical density measurement. *Mol. Ther.* **2003**, *7*, 122−128.
(31) Urabe, M.; et al. Scalable Generation of High-Titer Recombinant Adeno-Associated Virus Type 5 in Insect Cells. *J. Virol.* **2006**, *80*, 1874−1885.
(32) Kalambet, Y.; Kozmin, Y.; Mikhailova, K.; Nagaev, I.; Tikhonov, P. Reconstruction of chromatographic peaks using the exponentially modified Gaussian function. *J. Chemom.* **2011**, *25*, 352−356.
(33) Brusotti, G.; et al. Advances on Size Exclusion Chromatography and Applications on the Analysis of Protein Biopharmaceuticals and Protein Aggregates: A Mini Review. *Chromatographia* **2018**, *81*, 3−23.
(34) Wang, C.; et al. Developing an Anion Exchange Chromatography Assay for Determining Empty and Full Capsid Contents in AAV6.2. *Mol. Ther. - Methods Clin. Dev.* **2019**, *15*, 257−263.
(35) Sha, S.; et al. Cellular pathways of recombinant adeno-associated virus production for gene therapy. *Biotechnol. Adv.* **2021**, *49*, 107764.
(36) Nguyen, T. N. T.; et al. Mechanistic model for production of recombinant adeno-associated virus via triple transfection of HEK293 cells. *Mol. Ther. - Methods Clin. Dev.* **2021**, *21*, 642−655.

https://doi.org/10.1021/acs.nanolett.1c04092
Nano Lett. 2022, 22, 1511−1517